Molecular Therapy
Letter to the Editor

The Neurotropic Properties of AAV-PHP.B Are Limited to C57BL/6J Mice

Improved delivery of adeno-associated virus (AAV) vectors to the CNS will greatly enhance their clinical utility. Selection of AAV9 variants in a mouse model led to the isolation of a capsid called PHP.B, which resulted in remarkable transduction of the CNS following intravenous infusion. However, we now show here that this enhanced CNS tropism is restricted to the model in which it was selected, i.e., a Cre transgenic mouse in a C57BL/6J background, and was not found in nonhuman primates or the other commonly used mouse strain BALB/cJ. We also report the potential for serious acute toxicity in NHP after systemic administration of high dose of AAV.

Identification of adeno-associated virus (AAV) capsids from natural isolates with CNS tropism has substantially enhanced the utility of this platform for basic studies of neurobiology and therapeutic applications of gene therapy of CNS diseases.[1–3] The most widely used capsid for CNS applications has been AAV9, which we isolated from a human heart.[3] A number of groups have demonstrated distribution of transduction following systemic delivery of AAV9 into heart, skeletal muscle, and the CNS.[4–6] Clinical trials of systemically-delivered AAV9 are underway for targeting motor neurons of the spinal cord in patients with spinal muscular atrophy (ClinicalTrials.gov: NCT02122952) and in treating the neuropathic manifestations of the lysosomal storage disease Sanfilippo A (ClinicalTrials.gov: NCT02716246).

While AAV9 is unique compared to the many natural capsids that have been vectored in terms of CNS delivery, its efficiency is low even at very high systemic doses.[7] Deverman et al.[8] recently described an engineered variant of AAV9, called PHP.B, that exhibits much higher delivery to the CNS of mice following intravenous (i.v.) injection. This variant was isolated from a library of AAV9 capsids containing a randomized population of a 7 amino acid insert. A Cre transgenic line of C57BL/6J mice was used to select those capsid variants that efficiently trafficked to the CNS. PHP.B is being considered for the treatment of a wide range of CNS diseases.

In an attempt to develop PHP.B for human gene therapy, we evaluated its efficacy and toxicity in nonhuman primates (NHPs). Prior to doing so, we confirmed the findings of Deverman et al.[8] in C57BL/6J mice. Intravenous injection of 1E12 genome copies (GC) of PHP.B expressing GFP demonstrated remarkable transduction throughout the brain and the spinal cord, as measured by detection of GFP fluorescence, that was almost 4 logs higher than what was observed with AAV9 (Figures 1A and 1B; Figures S1 and S2). This high level of transduction was observed in multiple areas of the brain (Figure S2). Similar transduction was observed with both vectors in non-CNS tissues of C57BL/6J mice, such as liver and muscle (Figures 1A and 1B). Quantitation of vector genomes in tissue confirmed the substantially higher CNS gene transfer with PHP.B as described by Deverman et al.[8] (Figure 1C). We were surprised, however, with the results of the same experiment conducted in BALB/cJ mice, which showed very low transduction and gene transfer in the CNS that was no different than what was observed with AAV9 (Figures 1A–1C; Figures S1 and S2). Transduction and gene transfer of PHP.B was slightly lower than AAV9 in liver and muscle (Figures 1A–1C). For both vectors, transduction of liver and CNS was higher in C57BL/6J than in BALB/cJ, whereas muscle transduction was higher in BALB/cJ (Figures 1A–1C).

Despite the disappointing results obtained in BALB/cJ mice, we proceeded with pilot studies in NHPs (Table S1). Adult rhesus macaques (n = 1 per vector) that were negative for neutralizing antibodies to the respective capsids were injected with 2E13 GC/kg of the same GFP versions of AAV9 and PHP.B studied in mice; this represents a 2.5-fold lower vector per kg dose than we studied in mice, but it was also 4-fold higher than the low dose evaluated by Deverman et al.[8] that showed high-level CNS transduction in C57BL/6J mice. Both NHPs tolerated the vector well, with only minor abnormalities in clinical pathology (data not shown); both animals were necropsied at the planned time of 21 days. GFP expression was detected by direct fluorescence of GFP and quantified in most non-CNS tissues, including liver and muscle (Figures 2A and 2B), kidney, pancreas, heart, spleen, and pituitary (Figure S3) at equivalent levels in the AAV9- and PHP.B-treated animals, except for in skeletal muscle, where transduction was higher for PHP.B. However, very low transduction was observed in the CNS based on GFP fluorescence, including in the frontal cortex and spinal cord (Figures 2A and 2B) and hippocampus and cerebellum (Figure S3). Interestingly, the dorsal root ganglia (DRG), which lie outside of the CNS, were transduced at equally high levels with both AAV9 and PHP.B than were cells within the CNS (Figures 2A and 2B). The quantity of vector genomes in various tissues paralleled GFP expression (Figure 2C). Notably, vector genomes were 3 logs lower in tissues of the spinal cord and brain than in liver and spleen, with no differences between AAV9 and PHP.B.

Having demonstrated that both vectors were safe at 2E13 GC/kg, we injected animals (n = 1 per group) at a higher dose of 7.5E13 GC/kg. The animal injected with PHP.B vector developed marked elevations of serum transaminases along with profound thrombocytopenia and diffuse bleeding, which required euthanasia on day 5 (Figure 3; Table S2). Pathology at necropsy was consistent with diffuse hemorrhage (Figure S4). The AAV9-injected animal tolerated the vector well without clinical sequelae or laboratory abnormalities except biphasic elevations in transaminases, which were higher on day 14, presumably due to a T cell response to GFP (Figure 3; Table S2). Tissues were harvested on day 21 as planned and showed mild mononuclear cell infiltrates (Figure S5). A more thorough description of the clinical and laboratory abnormalities observed at high doses of vector can be found in the Supplemental Information.

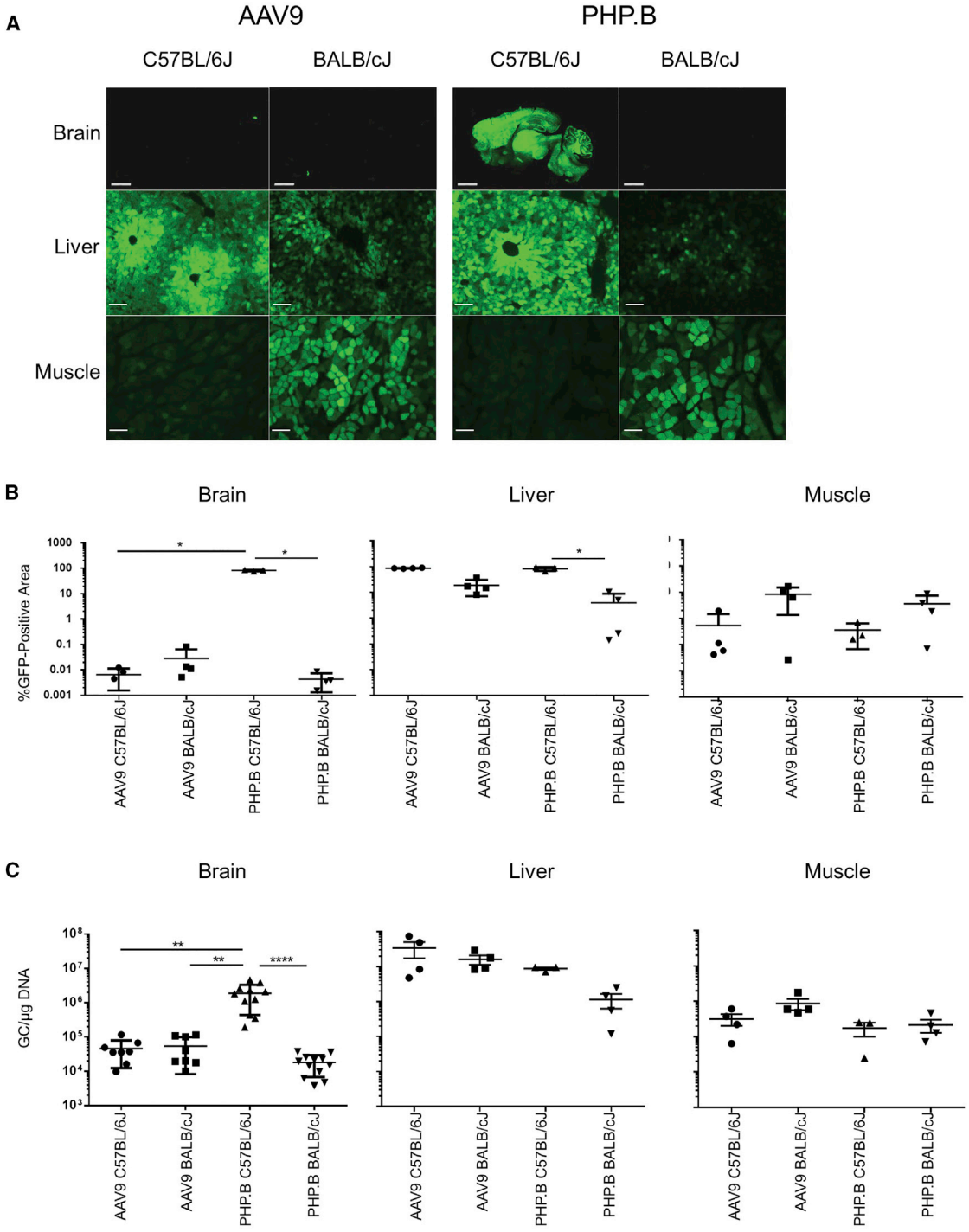

Figure 1. Comparison of AAV9- and PHP.B-Mediated Gene Transfer in Mice

(A) Direct GFP fluorescence in the brain, liver, and gastrocnemius muscle. Scale bars, 2 mm (brain) and 100 μm (liver, muscle). (B) GFP quantification of whole-slide scans. (C) Vector biodistribution in tissues. After systemic administration of 5E13 GC/kg to adult mice, PHP.B's ability to target the brain with high efficiency is limited to the C57BL/6J strain. In BALB/cJ adult mice, AAV9 and PHP.B are equivalent and display low blood-brain-barrier crossing. PHP.B-mediated brain transduction is intermediate in CB6F1 hybrids. *$p < 0.05$; **$p < 0.01$; ****$p < 0.0001$. Error bars represent SD.

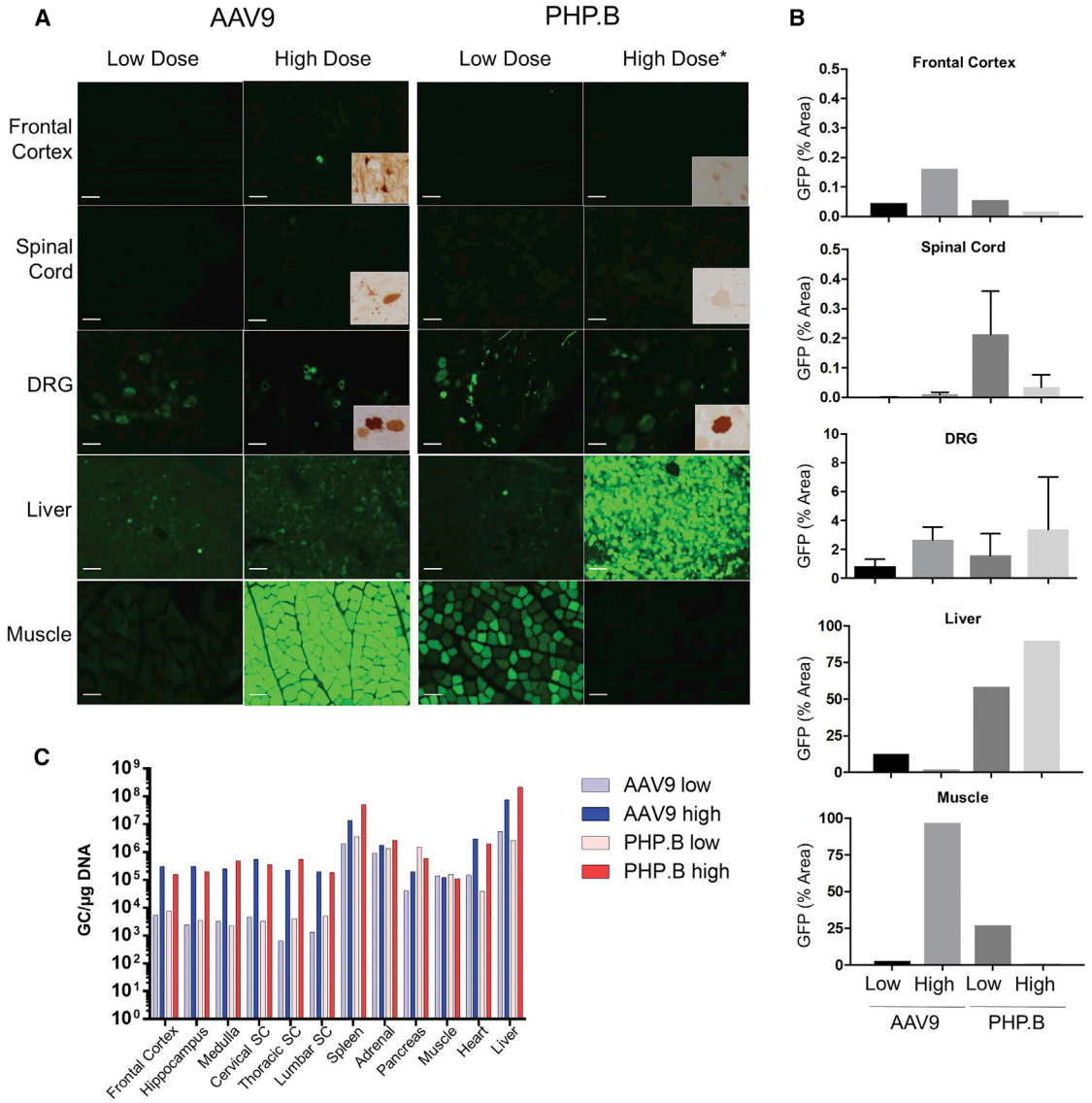

Figure 2. Comparison of AAV9- and PHP.B-Mediated Gene Transfer in Nonhuman Primates

(A) Direct GFP fluorescence in the cortex, spinal cord, dorsal root ganglia (DRG), liver, and quadriceps muscle. Insets show GFP immunohistochemistry in high-dose animals. *Euthanized 5 days post injection; all others were euthanized 21 days post injection. Scale bars, 100 µm. (B) GFP quantification showing values for whole-slide scans (cortex, liver, muscle) or averages and SD from multiple images taken with a microscope (10 images for DRGs, 2 images for lumbar spinal cord). (C) Vector biodistribution in tissues. After systemic administration of 2E13 GC/kg (low dose) or 7.5E13 GC/kg (high dose) to adult rhesus macaques, both AAV9 and PHP.B vectors are equivalent with low to mild CNS targeting. Organs unprotected by the blood-brain barrier, such as dorsal root ganglia, liver, and muscles, are efficiently transduced. Note that GFP expression is not directly comparable in the PHP.B high-dose monkey that was euthanized 5 days post injection due to vector-related clinical condition. Vector biodistribution is similar for dose-matched AAV9 and PHP.B vectors, showing that both vectors share the same tropism and properties in NHP.

The development of pathology in the PHP.B-treated animal and the different necropsy times make it difficult to compare the two high-dose animals in terms of transduction efficiency, although the amount of vector genomes measured in tissues were the same between the two animals and 2 to 3 logs higher in spleen and liver than in brain and spinal cord (Figure 2C). Very low to undetectable transduction, as measured by GFP fluorescence, was observed in CNS tissues, including frontal cortex and spinal cord (Figures 2A and 2B) and hippocampus and cerebellum (Figure S3). Like the low-dose animals, both high-dose animals demonstrated GFP expression in DRG (Figures 2A and 2B; Figure S6). Brain tissues from high-dose animals were also analyzed for GFP protein by immunohistochemistry, which confirmed the low transduction achieved with both vectors (high magnification insets in Figures 2 and S3 and low magnification micrographs in Figure S6). Expression of GFP outside of the CNS was

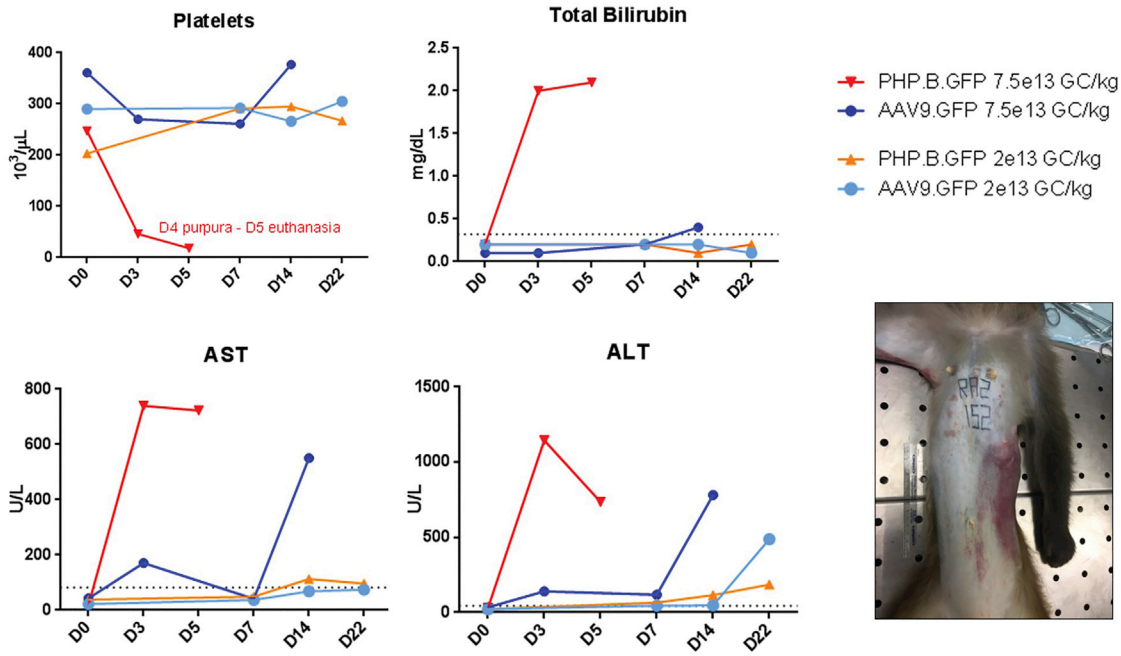

Figure 3. Toxicity Event in the High-Dose-Treated PHP.B NHP

Platelet counts, total bilirubin, transaminase levels, and gross picture of the cutaneous petechiae and bruises on the thorax and abdomen of the NHP treated with 7.5E13 GC/kg of PHP.B-GFP vector. The toxicity event was characterized by thrombocytopenia, hyperbilirubinemia, and increased transaminases on day 3 and day 5 post vector administration. Massive subcutaneous and internal bleeding led to humane euthanasia of the animal on day 5.

high, with substantial differences between the two vectors possibly reflecting the different times of necropsy and the influence of CTLs to transduce cells in the AAV9-treated animal that was necropsied at day 22 (Figures 2A and 2B; Figure S3). The level of transduction of skeletal muscle and heart achieved with the high-dose AAV9 vector was impressive, supporting its use in primary muscle diseases (Figures 2A and 2B; Figure S3). It is interesting that the amount of vector genomes was similar between the CNS and muscle in the AAV9 animal, although expression of GFP was logs higher in muscle.

We have never observed such a profound difference in AAV vector performance between two strains of mice. *In vivo* transduction of vectors based on natural isolates of AAV have generally tracked between strains of mice and different species, including larger animals, with the notable exception of liver, where mice are more efficiently transduced than primates.[9,10] The lack of translation from mice to NHPs and to humans is often explained by stronger immune responses in primates. Another team recently reported the lack of significant blood-brain barrier (BBB) penetration of PHP.B vector in a smaller NHP, the marmoset.[11] We do not think that stronger cell-mediated response in BALBc/J mice can explain the lack of GFP expression in the brain, as the liver was efficiently transduced and C57BL/6 and BALB/c mice are prototypical Th1- and Th2-type mouse strains, respectively, accounting for weak T cell responses in BALB/c.[12] The apparent restriction of high-CNS transduction with PHP.B to C57BL/6J mice may reflect the fact that it was selected for high delivery to the CNS in this strain of mice. This remarkable strain-specific difference in vector delivery to the CNS may facilitate the identification of factors that enhance CNS delivery.

We report an unprecedented acute toxicity event leading to the euthanasia of an NHP 5 days after injection. Clinical pathology, gross findings, and histology were compatible with acute tissue injury and systemic activation of innate immunity with endothelial cells and/or platelet activation, leading to consumption thrombocytopenia and secondary hemorrhages. While the event reported here has to be interpreted with caution due to the limited number of animals, the acute timing (within days after injection) suggests a direct AAV-mediated toxicity when administered i.v. at high doses that is different in timing, quality, and severity to the liver toxicity previously reported in systemic human AAV studies. In the systemic human AAV studies, the liver toxicity is believed to be caused by adaptive immune responses to the capsid or the transgene product. Additional NHP studies are needed to determinate the precise pathological and molecular mechanisms involved as well as the potential implication for clinical trials using comparable doses of systemic vectors. In the meantime, it seems prudent for sponsors to monitor acute manifestations of innate immunity, such as thrombocytopenia, in clinical trials involving high dose systemic AAV.

The low CNS transduction of PHP.B at doses of vector associated with dose-limiting toxicity in NHPs will limit its utility in

treating human diseases beyond that which could be achieved with AAV9.

SUPPLEMENTAL INFORMATION

Supplemental Information includes six figures, two tables, a clinical case description, and Supplemental Materials and Methods and can be found with article online at https://doi.org/10.1016/j.ymthe.2018.01.018.

AUTHOR CONTRIBUTIONS

J.H. designed and conducted mice and nonhuman primate studies and interpreted all the data. Q.W. produced the initial AAV-PHP.B vector and validated it *in vitro* and *in vivo*. N.K. conducted the initial experiment in BALB/cJ mice. E.L.B. analyzed histopathological and clinical data in nonhuman primates. P.B. supervised and analyzed GFP expression and quantification. J.M.W. conceived the studies, was responsible for research coordination and strategy, and wrote the manuscript. All authors discussed the results and commented on the manuscript.

CONFLICTS OF INTEREST

J.M.W. is an advisor to, a founder of, holds equity in, and has a sponsored research agreement with REGENXBIO; he is a former consultant to and holds stock in Solid Biosciences; he also has a sponsored research agreement with Ultragenyx; in addition, he is a consultant to several biopharmaceutical companies. J.M.W. is an inventor on patents licensed to various biopharmaceutical companies.

ACKNOWLEDGMENTS

We thank Cecilia Dyer, Mohamad Nayal, Vanitha Ramachandran, Tahsin Jahan, Liying Han, and Miao Jiang for invaluable technical assistance as well as the Program in Comparative Medicine and the Nonhuman Primate Research Program of the Gene Therapy Program at the University of Pennsylvania and the Human Immunology Core (P30-CA016520) for study support. Vectors were produced by the Penn Vector Core. We also thank Jennifer Stewart for editorial assistance with this manuscript.

Juliette Hordeaux,[1,2] Qiang Wang,[1,2] Nathan Katz,[1] Elizabeth L. Buza,[1] Peter Bell,[1] and James M. Wilson[1]

[1]Gene Therapy Program, Department of Medicine, Perelman School of Medicine, University of Pennsylvania, Philadelphia, PA, USA

https://doi.org/10.1016/j.ymthe.2018.01.018

[2]These authors contributed equally to this work.

Correspondence: James M. Wilson, MD, PhD, Gene Therapy Program, Department of Medicine, Perelman School of Medicine, University of Pennsylvania, 125 South 31st Street, Suite 1200, Philadelphia, PA 19104, USA.
E-mail: wilsonjm@upenn.edu

REFERENCES

1. Gao, G., Vandenberghe, L.H., and Wilson, J.M. (2005). New recombinant serotypes of AAV vectors. Curr. Gene Ther. *5*, 285–297.
2. Gao, G.P., Alvira, M.R., Wang, L., Calcedo, R., Johnston, J., and Wilson, J.M. (2002). Novel adeno-associated viruses from rhesus monkeys as vectors for human gene therapy. Proc. Natl. Acad. Sci. USA *99*, 11854–11859.
3. Gao, G., Vandenberghe, L.H., Alvira, M.R., Lu, Y., Calcedo, R., Zhou, X., and Wilson, J.M. (2004). Clades of Adeno-associated viruses are widely disseminated in human tissues. J. Virol. *78*, 6381–6388.
4. Duque, S., Joussemet, B., Riviere, C., Marais, T., Dubreil, L., Douar, A.M., Fyfe, J., Moullier, P., Colle, M.A., and Barkats, M. (2009). Intravenous administration of self-complementary AAV9 enables transgene delivery to adult motor neurons. Mol. Ther. *17*, 1187–1196.
5. Pacak, C.A., Mah, C.S., Thattaliyath, B.D., Conlon, T.J., Lewis, M.A., Cloutier, D.E., Zolotukhin, I., Tarantal, A.F., and Byrne, B.J. (2006). Recombinant adeno-associated virus serotype 9 leads to preferential cardiac transduction in vivo. Circ. Res. *99*, e3–e9.
6. Gray, S.J., Matagne, V., Bachaboina, L., Yadav, S., Ojeda, S.R., and Samulski, R.J. (2011). Preclinical differences of intravascular AAV9 delivery to neurons and glia: a comparative study of adult mice and nonhuman primates. Mol. Ther. *19*, 1058–1069.
7. Bevan, A.K., Duque, S., Foust, K.D., Morales, P.R., Braun, L., Schmelzer, L., Chan, C.M., McCrate, M., Chicoine, L.G., Coley, B.D., et al. (2011). Systemic gene delivery in large species for targeting spinal cord, brain, and peripheral tissues for pediatric disorders. Mol. Ther. *19*, 1971–1980.
8. Deverman, B.E., Pravdo, P.L., Simpson, B.P., Kumar, S.R., Chan, K.Y., Banerjee, A., Wu, W.L., Yang, B., Huber, N., Pasca, S.P., and Gradinaru, V. (2016). Cre-dependent selection yields AAV variants for widespread gene transfer to the adult brain. Nat. Biotechnol. *34*, 204–209.
9. Wang, L., Calcedo, R., Wang, H., Bell, P., Grant, R., Vandenberghe, L.H., Sanmiguel, J., Morizono, H., Batshaw, M.L., and Wilson, J.M. (2010). The pleiotropic effects of natural AAV infections on liver-directed gene transfer in macaques. Mol. Ther. *18*, 126–134.
10. Wang, L., Bell, P., Somanathan, S., Wang, Q., He, Z., Yu, H., McMenamin, D., Goode, T., Calcedo, R., and Wilson, J.M. (2015). Comparative Study of Liver Gene Transfer With AAV Vectors Based on Natural and Engineered AAV Capsids. Mol. Ther. *23*, 1877–1887.
11. Matsuzaki, Y., Konno, A., Mochizuki, R., Shinohara, Y., Nitta, K., Okada, Y., and Hirai, H. (2017). Intravenous administration of the adeno-associated virus-PHP.B capsid fails to upregulate transduction efficiency in the marmoset brain. Neurosci. Lett. *665*, 182–188.
12. Mills, C.D., Kincaid, K., Alt, J.M., Heilman, M.J., and Hill, A.M. (2000). M-1/M-2 macrophages and the

YMTHE, Volume *26*

Supplemental Information

The Neurotropic Properties of AAV-PHP.B Are Limited to C57BL/6J Mice

Juliette Hordeaux, Qiang Wang, Nathan Katz, Elizabeth L. Buza, Peter Bell, and James M. Wilson

Supplemental Data

Supplemental Figures

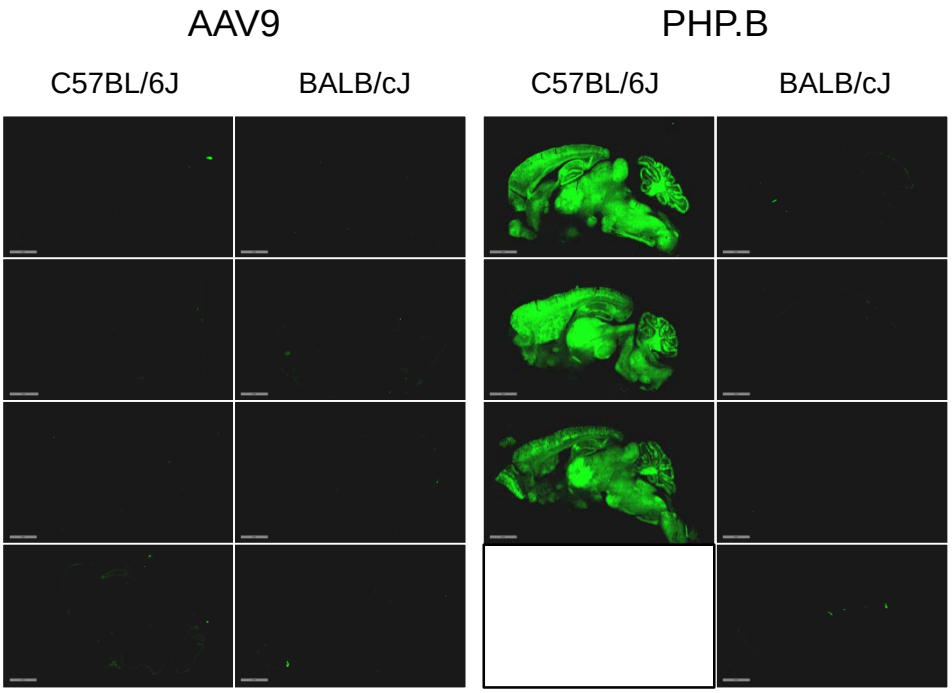

Supplemental Figure 1. Direct observation of GFP in the brain of individual AAV9 and PHP.B-injected mice. After systemic administration of $5x10^{13}$ GC/kg to adult mice, GFP expression is minimal in AAV9-injected mice and in PHP.B-injected BALB/cJ mice at 21 days post injection. GFP expression is marked in C57Bl6 PHP.B-injected mice.Individual variations are minimal. Data for one PHP.B-injected C57BL/6J animal is not available due to a failed injection. Scale bars 2mm.

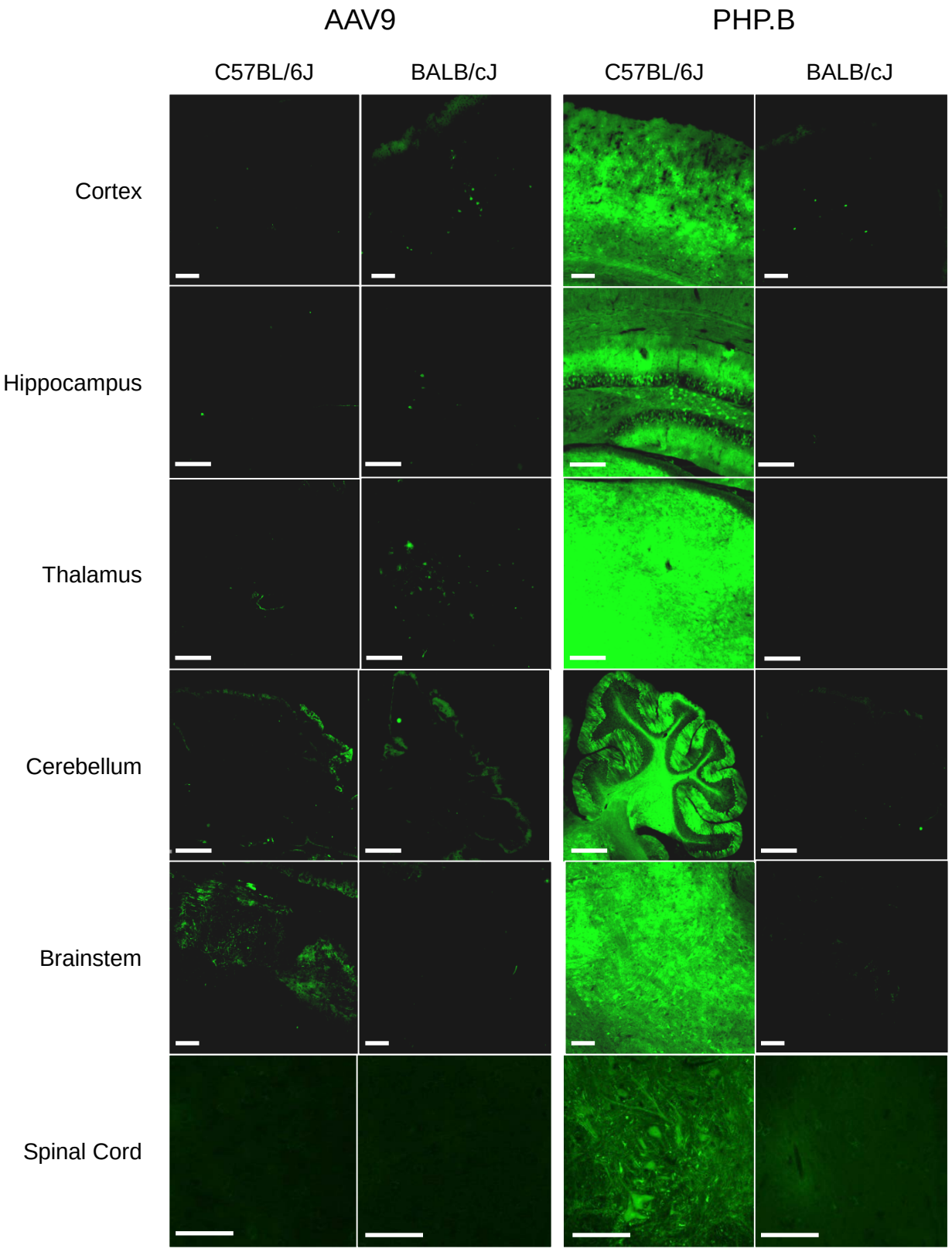

Supplemental Figure 2. Direct observation of GFP in the brain of AAV9 and PHP.B-injected mice at high magnification. Mice were injected in the tail vein with $5x10^{13}$ GC/kg of AAV9 or AAV-PHP.B encoding GFP. 21 days pi, all CNS regions are highly transduced after PHP.B injection in C57BL/6J mice: cortex (scale bar 100 µm), hippocampus (scale bar 200 µm), thalamus (scale bar 200 µm), cerebellum (scale bar 700 µm), brainstem (scale bar 150 µm), and spinal cord (motor neurons, scale bar 100 µm). PHP.B-driven GFP expression is marked in C57BL/6J and almost absent in BALB/cJ mice. With AAV9, no significant difference is seen in C57BL/6J and BALB/cJ mice.

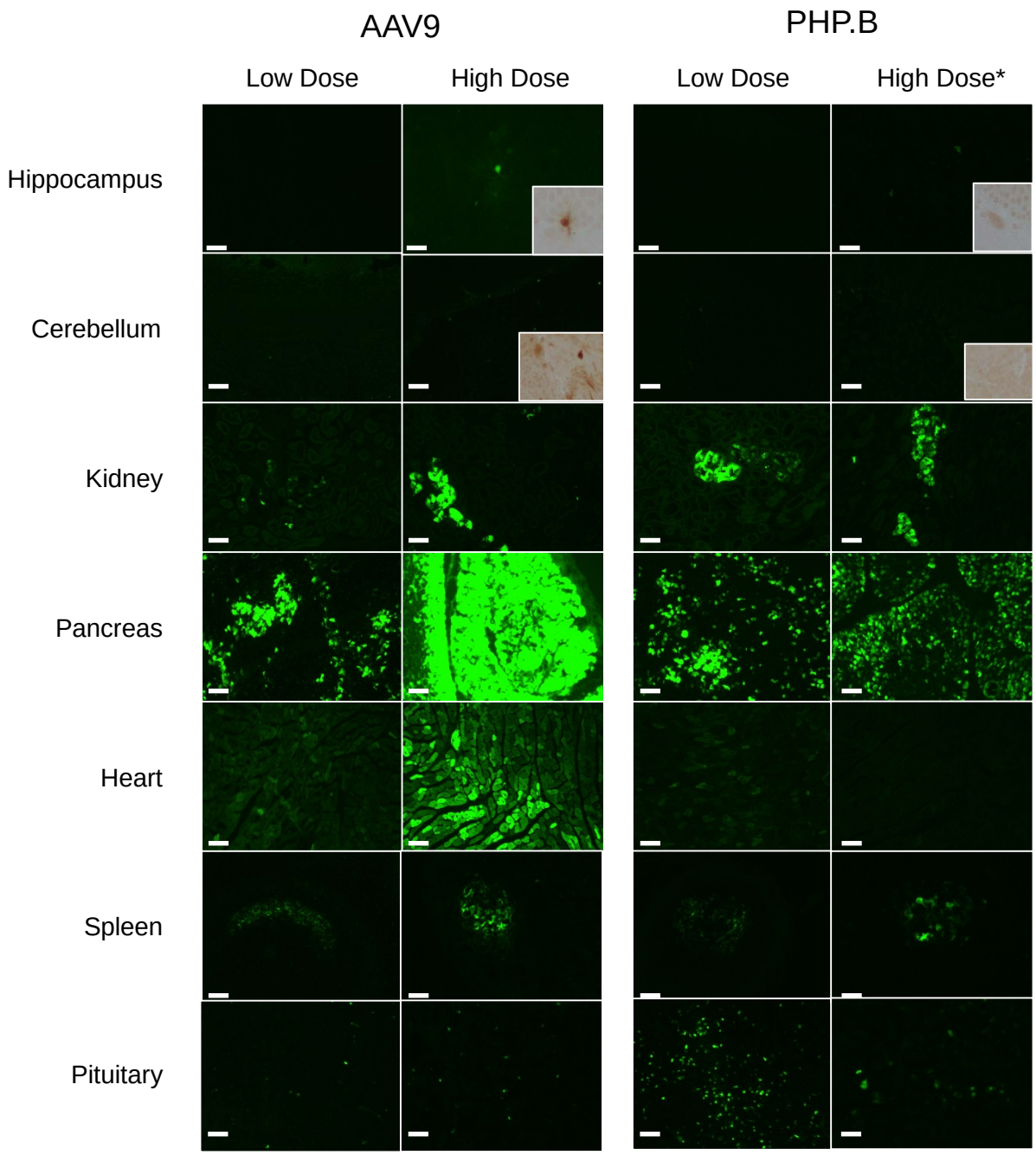

Supplemental Figure 3. AAV9 and PHP.B-mediated gene transfer in additional tissues of nonhuman primates. Low dose is $2x10^{13}$ GC/kg and high dose is $7.5x10^{13}$ GC/kg. Hippocampus, cerebellum, kidney, pancreas, heart, spleen, and pituitary are depicted. Inset images show GFP immunohistochemistry in the high dose animals. *Euthanized 5 days post injection; all others euthanized 21 days post injection. AAV9 drives dose-dependent GFP expression that is markedly more efficient in organs that lay outside of the blood-brain barrier. The expression profile is similar in PHP.B, although high-dose expression data are not directly comparable due to the shorter post injection time. Scales bars 100 µm.

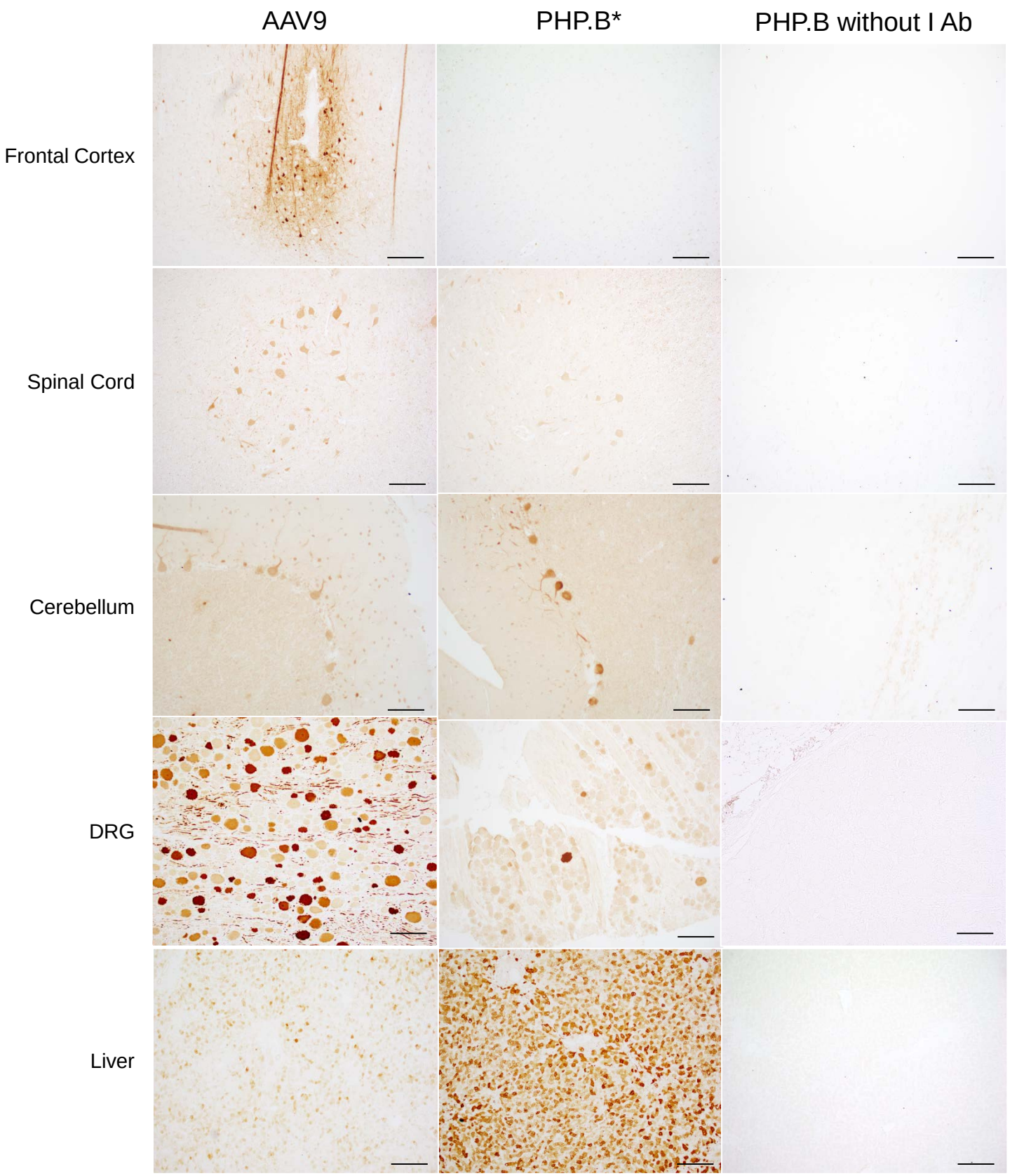

Supplemental Figure 4. GFP immunohistochemistry in high-dose nonhuman primates injected with AAV9 and PHP.B vectors. Frontal cortex, spinal cord (anterior horns), cerebellum, dorsal root ganglia (DRG), and liver are depicted. *Euthanized 5 days post injection. Positive (brown) neurons are seen in the AAV9 high-dose animal in the frontal cortex (perivascular pattern), anterior horns of the spinal cord, cerebellum (granular layer and Purkinje cells) and DRG. In the PHP.B animal, expression is suboptimal at this early timepoint and only visible in some Purkinje cells and DRG neurons. Scale bars 200 µm.

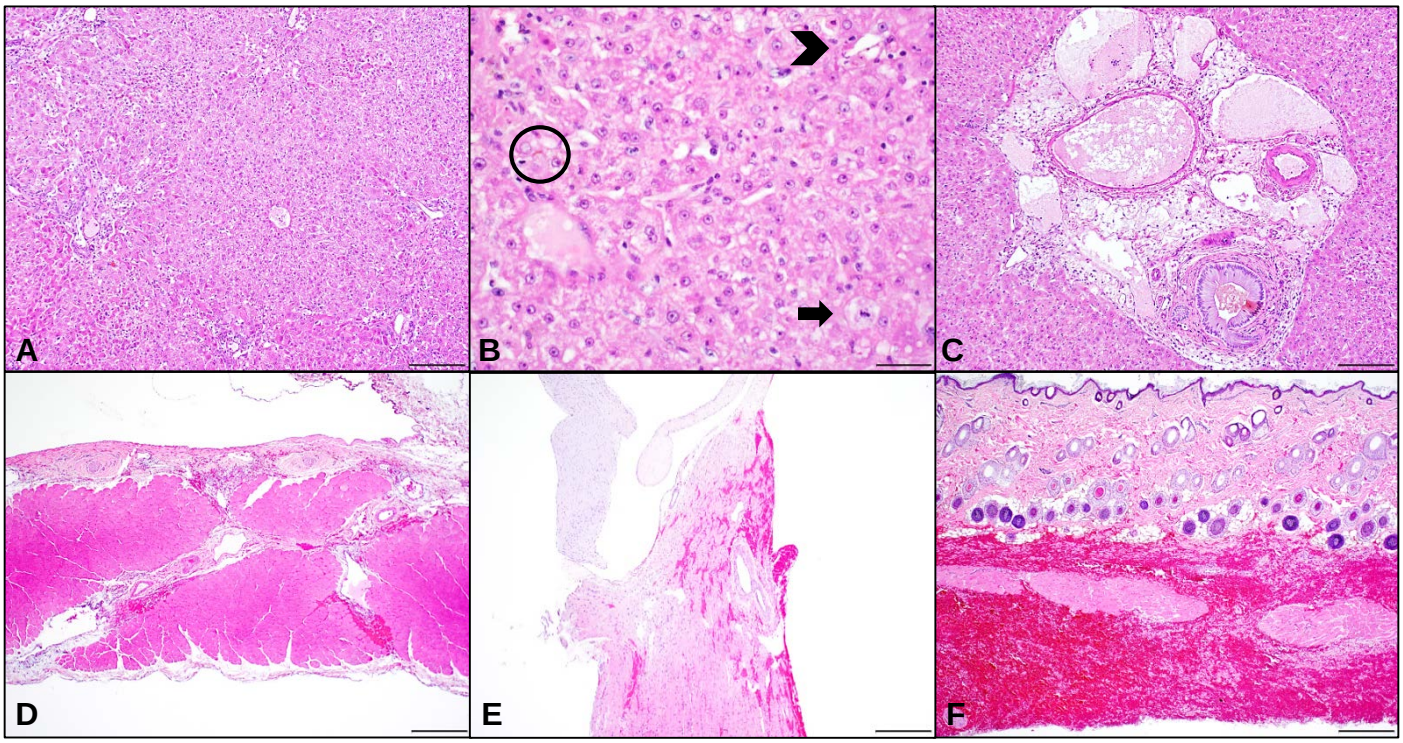

Supplemental Figure 5. Histopathology of high-dose PHP.B NHP (RA2152). The histology findings were most significant in liver (**A-C**) and consisted of marked multifocal single hepatocellular necrosis and degeneration, most prominently centered on portal regions with occasional bridging (**A**, scale bar 200 µm). Along with individual hepatocellular necrosis (*arrowhead*), there were also increased numbers of mitotic figures (*arrow*) indicative of regeneration (**B**, scale bar 50 µm). Both canalicular (**B**, circle) and ductal (**C**, scale bar 200 µm) bile stasis were prominent. Portal areas were edematous with dilated portal veins and lymphatics (**C**). Acute hemorrhage was observed in the diaphragm (**D**, scale bar 500 µm), heart (**E**, scale bar 500 µm), and subcutis (**F**, scale bar 200 µm).

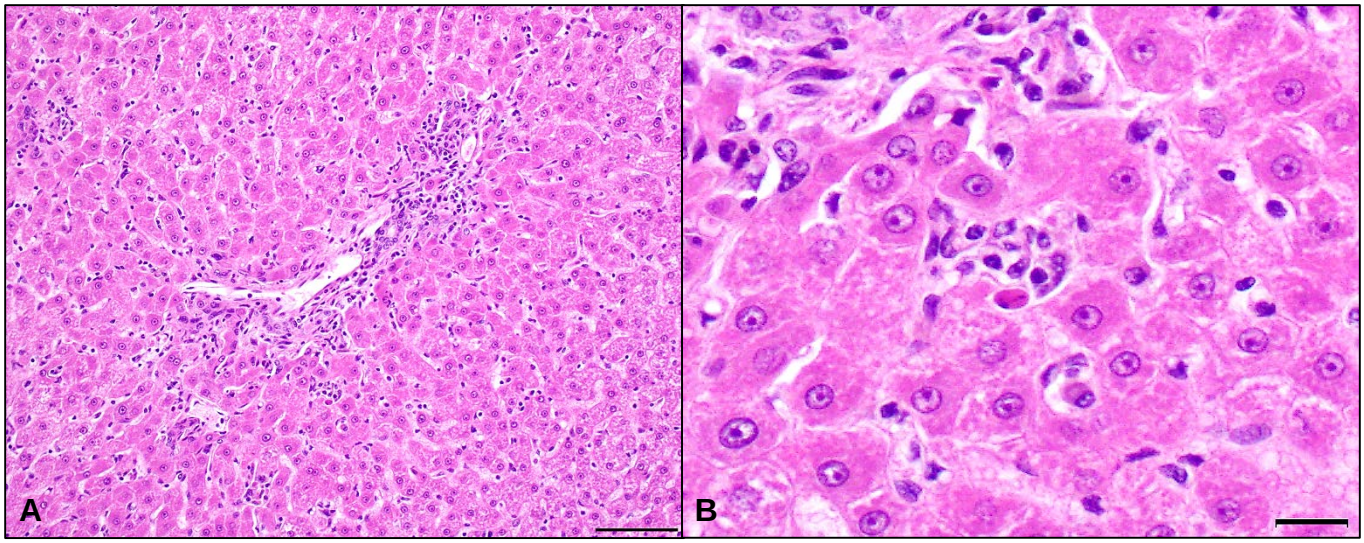

Supplemental Figure 6: Histopathology of high-dose AAV9 NHP (RA2235). The histopathology findings in animal RA2235 consisted of minimal mononuclear cell infiltrates within the liver (**A**-**B**). The mononuclear cell infiltrates in the liver were within portal and periportal areas (**A**, scale bar 100 µm) and occasionally associated with single hepatocellular necrosis (**B**, scale bar 20 µm). The mononuclear cell infiltrates likely corresponded to an immune (e.g. T-lymphocyte) response related to vector expression.

Supplemental Table 1. Nonhuman primates dosed with systemic AAV9 and PHP.B.

Animal	**Gender, age**	**Weight**	**Vector**		**Outcome**
RA2172	Female, 4 years	5.3 kg	AAV9.CB7.eGFP.WPRE.rBG	2e13 GC/kg	Scheduled euthanasia D21
RA2235	Male, 4 years	6.7 kg	AAV9.CB7.eGFP.WPRE.rBG	7.5e13 GC/kg	Scheduled euthanasia D21
RA2145	Female, 4 years	4.8 kg	AAV-PHP.B.CB7.eGFP.WPRE.rBG	2e13 GC/kg	Scheduled euthanasia D21
RA2152	Female, 4 years	5.9 kg	AAV-PHP.B.CB7.eGFP.WPRE.rBG	7.5e13 GC/kg	Hemorrhagic diathesis ; Unscheduled euthanasia D5

Supplemental Table 2. Clinical pathology, PHP.B (RA2152) and AAV9 (RA2235) high dose animals.

	Parameter	Day 0, prior to dosing	Day 3	Day 5	Day 7	Day 14	Day 21
RA2152 PHP.B	White blood cells 10^3/µL	12.2	3	3.8	N/A	N/A	N/A
	Red blood cells 10^6/µL	4.5	4.8	3			
	Hemoglobin g/dL	11.6	12.5	7.3			
	Hematocrit %	38	37	23			
	Mean corpuscular volume fl/cell	85	77	75			
	Mean corpuscular hemoglobin pg/cell	25.6	26.2	24.2			
	Mean corpuscular hemoglobin g/dL	30	34	32			
	Platelets 10^3/µL	247	46	18			
	Neutrophils cell/µL	8,662	1200	1748			
	% neutrophils	71	40	46			
	Bands cell/µL	0	0	0			
	% band cells	0	0	0			
	Lymphocytes cell/µL	2,928	1,710	1,368			
	% Lymphocytes	24	57	36			
	Monocytes cell/µL	244	60	380			
	% monocytes	2	2	10			
	Eosinophils cell/µL	366	30	304			
	% eosinophils	3	1	8			
	Basophils cell/µL	0	0	0			
	% basolphils	0	0	0			
	Total protein g/dL	6.6	5.9	5.3			
	Albumin g/dL	4.2	3.2	3			
	Globulin g/dL	2.4	2.7	2.3			
	A\G ratio	1.8	1.2	1.3			
	AST IU/ L	19	740	242			
	ALT IU/ L	30	1,145	736			
	ALP IU/ L	311	680	723			
	GGTP IU/ L	61	123	90			
	Total bilirubin mg/dL	0.2	2	2.1			
	Urea (BUN) mg/dL	17	17	14			
	Creatinine mg/dL	0.5	0.4	0.3			
	BUN/CREA Ratio	34	43	47			
	Ph mg/dL	5.3	4.5	4			
	Glucose mg/dL	57	92	77			
	Ca mg/dL	9.2	7.9	7.9			
	Mg mg/dL	1.5	1.8	1.6			
	Na mmol/L	145	139	141			
	K mmol/L	3.1	3.6	4.2			
	NA/K ratio	47	39	34			
	Chloride mmol/L	108	105	106			
	Cholesterol	117	99	108			
	Triglycerides	49	19	27			
	Amylase U/L	304	194	248			
	Precision Pancreas specific lipase U/L	29	26	18			
	Creatine phosphokinase U/L	535	124	857			
	Prothrombin time sec	9.5	11.9	12			
	Partial thromboplastin time sec	25.4	31.5	29.8			
	Fibrinogen mg/dL	136	134	79			
	D-dimer ng/mL	42	147	20			
RA2235 AAV9	White blood cells 10^3/µL	7.2	7	N/A	12	6.3	6
	Red blood cells 10^6/µL	5.7	5.4		5.6	5.6	5.3

	Hemoglobin g/dL	13.1	12.9		12.8	12.6	12.4
	Hematocrit %	46	42		43	44	41
	Mean corpuscular volume fl/cell	80	77		76	78	78
	Mean corpuscular hemoglobin pg/cell	23	23.7		22.8	22.7	23.5
	Mean corpuscular hemoglobin g/dL	29	31		30	29	30
	Platelets 10^3/µL	361	270		261	377	428
	Neutrophils cell/µL	3168	3640		5160	2898	1260
	% neutrophils	44	52		43	46	21
	Bands cell/µL	0	0		0	0	0
	% band cells	0	0		0	0	0
	Lymohocytes cell/µL	3672	3290		5760	2898	4140
	% Lymphocytes	51	47		48	46	7
	Monocytes cell/µL	288	70		840	441	420
	% monocytes	4	1		7	7	7
	Eosinophils cell/µL	72	0		240	63	180
	% eosinophils	1	0		2	1	3
	Basophils cell/µL	0	0		0	0	0
	% basolphils	0	0		0	0	0
	Total protein g/dL	6.5	6.6		6.4	6.2	5.9
	Albumin g/dL	4.4	3.9		3.9	3.9	3.7
	Globulin g/dL	2.1	2.7		2.5	2.3	2.2
	A\G ratio	2.1	1.4		1.6	1.7	1.7
	AST IU/ L	43	171		41	551	54
	ALT IU/ L	34	140		118	782	231
	ALP IU/ L	608	574		508	640	748
	GGTP IU/ L	77	85		80	135	142
	Total bilirubin mg/dL	0.1	0.1		0.2	0.4	0.3
	Urea (BUN) mg/dL	22	19		19	18	17
	Creatinine mg/dL	0.6	0.6		0.6	0.6	0.5
	BUN/CREA Ratio	37	32		32	30	34
	Ph mg/dL	7.1	6.1		5.6	6.8	6.3
	Glucose mg/dL	75	144		118	76	98
	Ca mg/dL	9.3	9.4		9.1	9	9.7
	Mg mg/dL	1.6	1.5		1.5	1.4	1.4
	Na mmol/L	146	141		143	147	144
	K mmol/L	3.9	4.1		2.8	3.7	3.7
	NA/K ratio	37	34		51	40	39
	Chloride mmol/L	108	107		107	107	106
	Cholesterol	137	126		139	142	175
	Triglycerides	51	138		73	50	137
	Amylase U/L	262	258		283	204	258
	Precision Pancreas specific lipase U/L	45	44		34	29	36
	Creatine phosphokinase U/L	2383	141		123	171	134
	Prothrombin time sec	10	9.4		8.4	10.4	10.5
	Partial thromboplastin time sec	24.4	23.1		22.5	23.4	25.8
	Fibrinogen mg/dL	181	224		198	170	116
	D-dimer ng/mL	41	47		24	92	67

N/A not applicable

Clinical Case Description

A summary of the clinical findings for NHPs that received 7.5E13 GC/kg of AAV9 or PHP.B is provided below. Test article (AAV-PHP.B.CB7.CI.eGFP.WPRE.rBG; group 2) or reference article (AAV9.CB7.CI.eGFP.WPRE.rBG; group 1) was administered at a dose of 7.5E13 GC/kg IV to rhesus macaques (*Macaca mulatta*), RA2152 and RA2235, respectively (Supplemental Table 1). Necropsies were scheduled for 21 ±1 days post vector administration; however, animal RA2152 (PHP.B; group 2) was euthanized on Day 5 due to clinical signs and bloodwork abnormalities. Subsequently, direct histological comparison of these 2 vectors was not possible. The clinical pathology data for both animals are depicted in Supplemental Table 2.

Animal RA2235 (group 1), which received AAV9, was clinically normal throughout the study and necropsied according to protocol on Day 22. Grossly, no significant study-related findings were observed. No significant abnormalities were noted on serial complete blood counts (CBC); however, serum chemistry on Day 3 showed elevated (~200 U/L) liver enzymes (AST/ALT) and were trending down until Day 14. On Day 14, aspartate aminotransferase (AST) and alanine aminotransferase (ALT) spiked to ~500-800 U/dL and returned to normal levels by Day 22. Histologically within the liver there was minimal mononuclear cell infiltrates, primarily within portal and periportal regions that were occasionally associated with single hepatocellular necrosis (Supplemental Fig. 6). Minimal to mild mononuclear cell infiltrates were also observed in the heart and skeletal muscle of the diaphragm, right biceps brachii, right quadriceps femoris, and left gastrocnemius muscles (data not shown). Given the level of GFP expression in the heart and skeletal muscle, an association between these infiltrates and AAV9 vector cannot be completely ruled out; however, similar infiltrates have been reported as incidental or background findings in nonhuman primates[1]. However, the lack of concurrent sham-treated control animals renders the interpretation of these infiltrates difficult. Additionally, minimal multifocal perivascular mononuclear cell infiltrates were in brain, and the relationship of these findings to the reference article was uncertain. The dorsal root ganglia (DRG) had minimal mononuclear cell infiltrates with occasional neuronal cell body degeneration; however, all spinal cord segments were histologically unremarkable.

Animal RA2152 (group 2), which received PHP.B, had icteric serum on Day 3 and serum chemistry revealed an elevated AST (740 IU/L; x40 baseline), ALT (1,145 IU/L; x40 baseline) and total bilirubin (2 mg/dL; x10 baseline). On complete blood count (CBC), leukopenia ($3x10^3$/uL; x4 decrease / baseline) and thrombocytopenia ($46x10^3$/uL; x5 decrease / baseline) were noted. D-dimers (147 ng/dL) were increased on coagulation panel relative to baseline (Day 0, 42 ng/mL). Prothrombin time (PT, 11.9 sec) and partial thromboplastin time (PTT; 31.5 sec) were slightly increased compared to baseline (Day 0, PT 9.5 sec and PTT 25.4 sec); however, they were within reference range. Although behaviorally normal, the animal received IV fluids, preventative anti-emetic, and corticosteroids. On Day 4, petechial to ecchymotic to suffusive cutaneous hemorrhage was noted on the ventral and lateral abdomen and by Day 5 spread from the ventral abdomen to the left dorsum and right axillary region. While behaviorally normal, the animal was euthanized on Day 5 according to study protocol due to worsening cutaneous hemorrhage and anemia (HCT 20%), which was possibly indicative of bleeding to a coagulopathy. In addition to the skin lesions, the abdominal cavity contained approximately 30-35 mL of serosanguineous fluid. The cranial and caudal mediastinum along with the abdominal mesentery contained regional acute hemorrhage. The liver was diffusely tan and friable with an accentuated lobular pattern. Terminal clinical pathology (Day 5) data revealed a marked thrombocytopenia and stable leukopenia. Serum chemistry showed improvement of liver enzymes (AST 242 IU/L and ALT 736 IU/L) and stable total bilirubin (2.1 mg/dL). PT and PTT remained stable on coagulation panel; however, fibrinogen (79 mg/dL) was decreased compared to baseline (Day 0, 136 mg/dL) and Day 3 (134 mg/dL). The histologic findings consisted of acute hemorrhage within the diaphragm, heart, and subcutis (Supplemental Fig. 5). The gross lesions within the liver corresponded histologically to marked multifocal single hepatocellular necrosis and degeneration, most prominently centered on portal regions with occasional bridging. The necrotic hepatocytes were occasionally clustered into small aggregates. The portal areas were edematous with dilated portal veins and lymphatics. Bile ducts contained inspissated bile along with prominent canalicular bile plugs, indicative of cholestasis. Throughout

the hepatic parenchyma, there were increased numbers of mitotic figures, consistent with regeneration. No significant cellular infiltrates were observed in the liver or any other tissue examined.

A Luminex cytokine panel on serum from animal RA2152 showed no significant elevations for the majority of cytokines, except vascular endothelial growth factor (VEGF; Day 7, x10) and monocyte chemoattractant protein-1 (MCP-1; Day 3, x2). The Luminex results are not supportive of a systemic inflammatory or innate immune response; however, the treatment with corticosteroids (Day 3; 10 mg/kg) may have had an effect. Neutralizing antibody (NAb) titers for anti-AAV9/anti-PHP.B were performed for both animals. Baseline AAV9 neutralizing antibody titers were below the limit of detection (< 1:5) for both animals, while PHP.B total binding antibody titer was 1:800 for animal RA2152 and 1:40 for animal RA2135.

While the inciting cause of morbidity in animal RA2152 was likely vector-related, the mechanism is not well understood. Proposed pathologic mechanisms include primary liver injury due to AAV particles or genomes or cytokine-induced endothelial cell activation within the liver microvasculature with subsequent coagulation activation, and/or localized antigen-antibody sinusoidal endothelial cell injury. Other possibilities including systemic inflammatory conditions such as systemic endothelial activation/damage or antigen-antibody mediated platelet destruction. Individual genetic variability likely played a role as animal RA2145 (low dose, 2E13 GC/kg, PHP.B) had a similarly high vector genome distribution to the liver but did not experience significant liver injury or endothelial cell activation. While both animals were negative for NAbs to the respective vectors prior to treatment, the level of binding antibody to PHP.B in animal RA2152 was higher than binding antibody to AAV9 in RA2235. It is possible that AAV immune complexes caused by the higher binding antibodies in RA2152 may have contributed to toxicity.

Materials and Methods

Vectors

EGFP was cloned into an expression construct containing a chicken β-actin promoter, cytomegalovirus (CMV) enhancer, intron, and rabbit β-globin (rBG) polyadenylation sequence. The expression constructs were flanked by AAV2 inverted terminal repeats. The PHP.B *trans* plasmid[2] was constructed with QuikChange Lightning Site-Directed Mutagenesis Kit (Agilent Technologies, CA) on AAV9 trans plasmid. AAV vectors were manufactured by Penn Vector Core with iodixanol gradient method.[3] The purified vectors were titrated 3 times with Droplet Digital PCR[4] plus proteinase K pre-treatment, and the average of the 3 titers was used. The lots injected to NHPs had a purity of 100% and undetected endotoxin levels (<1.0 EU/mL).

Animal Procedures and Histology

All animal protocols were approved by the Institutional Animal Care and Use Committee of the University of Pennsylvania. C56BL/6J (stock #000664), BALB/cJ (#000651), and CB6F1/J (#100007) were purchased from The Jackson Laboratory. Mice received 1×10^{12} GC (5×10^{13} GC/kg) of AAV9 or PHP.B in 0.1 mL via the lateral tail vein and were euthanized by inhalation of CO_2 21 days post injection. Tissues were promptly collected, half was snap-frozen on dry ice (biodistribution), and half was immersion-fixed in 10% neutral formalin, cryo-preserved in sucrose, frozen in OCT, and sectioned with a cryostat for GFP direct observation and whole-slide scanning for GFP quantification. Four mice of each strain were injected with each vector and used for quantification of vector genome and GFP expression in tissues. A total of 8 AAV9 C57BL/6J, 8 AAV9 BALB/cJ, 12 PHP.B C57BL/6J, 12 PHP.B BALB/cJ, and 4 PHP.B CB6F1/J were used for the quantification of genome copies in the brain.

Adult (4 years old) rhesus macaques were purchased from Covance (Table S1). They received 2×10^{13} GC/kg (low dose, n = 1 per vector) or 7.5×10^{13} GC/kg (high dose, n = 1 per vector) of AAV9 or PHP.B in 10 mL via the saphenous vein under sedation (intramuscular dexmedetomidine with ketamine). All but one animal (see clinical case description) was euthanized 21 days post injection by barbiturate overdose after anesthesia. The PHP.B high-dose animal was euthanized due to clinical condition 5 days post injection. Tissues were promptly collected, some were snap-frozen on dry ice (biodistribution), and some were immersion-fixed in 10% neutral formalin, cryo-preserved in sucrose, frozen in OCT, and sectioned with a cryostat for GFP direct observation and whole-slide scanning for GFP quantification. In addition, tissues were sampled for paraffin embedding, H&E staining, and GFP immunohistochemistry in the 2 high-dose animals.

GFP Expression

To observe direct GFP fluorescence, tissue samples were fixed in formalin for about 24 hr, briefly washed in PBS, equilibrated sequentially in 15% and 30% sucrose in PBS until sinking to the bottom of the container, and finally frozen in OCT embedding medium for the preparation of cryosections. Sections were mounted in Fluoromount G containing DAPI (Electron Microscopy Sciences, Hatfield, PA) as nuclear counterstain.

GFP immunohistochemistry was performed on paraffin-embedded tissue samples. Sections were deparaffinized with ethanol and xylene, boiled for 6 min in 10 mM citrate buffer (pH 6.0) for antigen retrieval, treated sequentially with 2% H_2O_2 (15 min), avidin/biotin blocking reagents (15 min each; Vector Laboratories, Burlingame, CA), and blocking buffer (1% donkey serum in PBS + 0.2% Triton for 10 min), and followed by incubation with primary (1 hr) and biotinylated secondary antibodies (45 min; Jackson Immunoresearch, West Grove, PA) diluted in blocking buffer. As primary antibody served a rabbit serum against GFP (ab6556; Abcam, Cambridge, MA). A Vectastain Elite ABC kit (Vector Laboratories) was used following the manufacturer's instructions, with DAB as substrate, to visualize bound antibodies as brown precipitate.

Images were taken either with a Nikon Eclipse Ti-E microscope or, for low magnification pictures, as screen shots from slides scanned with an Aperio Versa fluorescence slide scanner (Leica Biosystems).

GFP Quantification

Slides of mice whole-brain, nonhuman primate frontal cortex, liver, and muscle containing cryosections were scanned with a 10× objective using an Aperio Versa fluorescence slide scanner (Leica Biosystems). Nonhuman primate DRG and lumbar spinal cord section images (10 for DRGs and 2 for lumbar spinal cord cross sections) were taken using a fluorescent microscope (Nikon Eclipse Ti-E microscope). The resulting image files were analyzed for fluorescence intensity and percentage of GFP^+ area using Halo software (Indica Labs, Corrales, NM). Briefly,

regions of interest comprising either whole sections or certain brain regions were drawn with Halo, and a threshold was set for GFP^+ areas. A comparison to control images taken with a red filter set was used to control for autofluorescence. Identical settings were used between animal groups for a given organ.

H&E staining was performed according to standard protocols on paraffin sections.

Vector Biodistribution

Tissue DNA was extracted with QIAamp DNA Mini Kit (QIAGEN, CA), and vector genomes were quantified by real-time PCR using Taqman reagents (Applied Biosystems, Life Technologies, CA) and primer/probe targeting the rBG polyadenylation sequence of the vectors.

Statistics

GFP quantification results and vector genome copies in mice were analyzed using one-way ANOVA (Kruskal Wallis test) followed by Dunn's multiple comparisons test with an alpha value of 0.05 (GraphPad Prism).

Supplemental References

1. Patrick, D, and Rebelatto, M (2015). Toxicologic pathology and background lesions of nonhuman primates In: Bluemel, J, Korte, S, Schenck, E and Weinbauer, G (eds). *The Nonhuman Primate in Nonclinical Drug Development and Safety Assessment*. G. Elsevier. pp 245-252.
2. Deverman, B.E., Pravdo, P.L., Simpson, B.P., Kumar, S.R., Chan, K.Y., Banerjee, A., Wu, W.-L., Yang, B., Huber, N., Pasca, S.P., and Gradinaru, V.ea (2016). Cre-dependent selection yields AAV variants for widespread gene transfer to the adult brain. Nat Biotechnol. 34, 204–209 34.
3. Lock, M., Alvira, M., Vandenberghe, L.H., Samanta, A., Toelen, J., Debyser, Z., and Wilson, J.M. (2010). Rapid, simple, and versatile manufacturing of recombinant adeno-associated viral vectors at scale. Hum. Gene Ther. 21, 1259–1271.
4. Lock, M., Alvira, M.R., Chen, S.J., and Wilson, J.M. (2014). Absolute determination of single-stranded and self-complementary adeno-associated viral vector genome titers by droplet digital PCR. Hum. Gene Ther. Methods 25, 115–125.